Leakage Error Compensation in Motor Current Signature Analysis for Shaft Misalignment Detection in Submersible Pumps

Nurafnida Afrizal, Roberto Ferrero, *Senior Member, IEEE*

***Abstract*—Excessive vibrations in motor operation can be a cause of premature failure in many industrial applications; therefore, effective solutions to accurately measure vibrations are required. A common approach to measure vibrations is through the motor current signature analysis, as torque oscillations produce characteristic frequency components in the current spectrum; this approach is suitable for those industrial applications where the rotating parts are not directly accessible for sensor installation, e.g. electrical submersible pumps which are usually deep underground or underwater. The detection of vibrations from the current spectrum is particularly challenging in high-power motors, where the ratio between the amplitude of the side-band spectral components caused by vibrations and the amplitude of the fundamental component is so small that the former is likely to be masked by the spectral leakage of the latter when a traditional Fourier analysis is employed. This paper proposes a method to improve the side-band amplitude measurement by compensating for the leakage error in the current spectrum. The method is applied, in particular, to the detection of vibrations caused by a shaft angular misalignment, but it can be applied to other types of vibrations as well. The method is firstly illustrated through simulation results and then experimentally validated on a smaller-scale motor. Results confirm the ability of the proposed method to accurately measure the side-band amplitude even when it was originally completely hidden by the spectral leakage of the fundamental component.**

***Index Terms*—Induction motors, Condition monitoring, Vibration measurement, Current measurement, Signal processing algorithms, Frequency-domain analysis**

I. Introduction

The operation of electric motors, like all other rotating machines, is likely to be characterized by some kind of vibrations, which can originate from a number of factors in the mechanical construction of the motor itself, in the connection to the load or in the electrical supply. While low levels of vibrations can be tolerated in most industrial applications, excessive vibrations for prolonged periods of time can damage the mechanical parts of the motor and the load, and can lead to a premature failure.

The need for an effective monitoring of motor vibrations has therefore attracted significant research efforts for the last decades, resulting in a vast literature on the subject. The most common monitoring solutions are based on mechanical measurements (typically by accelerometers) [1], [2], on electrical measurements (typically motor current signature analysis) [3]–[8], or in some cases on acoustic measurements [9]–[11]. Motor current measurements are particularly convenient because they do not require sensors placed on or near the motor itself, and they can often be performed by using the current sensors already installed for the control of the motor.

The motor current signature analysis for vibration monitoring is based on the fact that vibrations cause torque oscillations that are reflected into oscillations in the absorbed current, whose frequency depends on the type of vibration. The analysis of the current spectrum in the frequency domain can therefore reveal frequency components that are associated with specific vibration modes, and whose amplitude can be used to estimate the extent of the vibration that caused them. It should be noted, however, that the amplitude of those side-band frequency components in the current spectrum is usually orders of magnitude smaller than the amplitude of the main component (the higher the motor power, the larger the difference). Their accurate measurement is therefore hindered by the spectral leakage from the main component, which is likely to occur due to non-synchronous sampling, caused in turn by the time-varying nature of the electrical frequency. In this case, a standard Fourier analysis is no longer suitable, and more advanced signal processing methods are required to accurately estimate the amplitude of the side-band frequency components in the current spectrum.

A number of possible methods have been developed to deal with the time-frequency analysis of non-stationary signals, such as the Short-Time Fourier Transform, Wavelet Transform, Hilbert Transform and Taylor-Fourier Transform [3], [5]–[7], [12]–[14]. They have different features that make them suitable for different types of applications, but in general they are convenient for the analysis of signals characterized by several frequency components (often *a priori* unknown), with significant transients in their amplitudes and/or frequencies. The computational burden is often quite heavy, and the interpretation of the results is not always straightforward. The problem considered here is, on the contrary, conceptually simpler. Only a small number of well-defined frequency components appear in the current spectrum, and their expected frequencies are known *a priori*, with only small variations over time, which can be neglected if a reasonably short time window is considered for the observation of the signal. Therefore, a traditional Fourier analysis may still be appropriate on such a

N. Afrizal is with the Department of Electrical Engineering and Electronics, University of Liverpool, Liverpool L69 3GJ, UK, and with School of Ocean Engineering, Universiti Malaysia Terengganu, Malaysia (e-mail: Nurafnida.Afrizal@liverpool.ac.uk, nurafnida@umt.edu.my).

R. Ferrero is with the Department of Electrical Engineering and Electronics, University of Liverpool, Liverpool L69 3GJ, UK (e-mail: Roberto.Ferrero@liverpool.ac.uk).

short time window, provided that the spectrum can be cleaned from the spectral leakage.

The most common approach to decrease spectral leakage in non-synchronous sampling conditions is based on the use of non-rectangular windows, such as the cosine windows [15]. However, a n-th order window requires a n-times longer observation time for a given frequency resolution in the spectrum or, vice-versa, it enlarges the frequency resolution by n times for a given observation time and may even increase the leakage as a consequence of this. Hence, non-rectangular windows are not the most appropriate solution in the considered application, which requires at the same time short time windows to avoid transients and good frequency resolution to detect specific side-bands.

The aim of this paper is to present a signal processing method for the motor current signature analysis in the frequency domain that compensates for the leakage error arising from a non-synchronous sampling of the dominant current component at the electrical frequency, based on *a priori* information about the signal. This allows an accurate detection of vibration levels even when the effect on the current spectrum is very small and invisible with a standard Fourier analysis. A similar method was initially employed in [16], for the detection of broken rotor bar faults in induction motors, which create quite large vibrations and associated large side-band components in the current spectrum. Here, the same underlying idea is applied to detect much smaller side-band components, created by small vibrations that do not qualify as faults but may lead to faults in the long term. Such a different level of vibrations creates additional challenges, which are addressed in this paper, with reference to a specific case study of practical relevance.

A particularly interesting industrial application for the proposed method is the condition monitoring of Electrical Submersible Pumps (ESPs), whose vibration monitoring is at the same time very important and very challenging to achieve. On the one hand, some critical pump components, such as the mechanical seal, are very sensitive to vibrations and are likely to fail prematurely in case of excessive vibrations, with huge economic implications, due to the operation downtime and the cost of replacement. On the other hand, the vibration monitoring is hindered by the fact that the pump and the motor are submerged, often at very large depth underground or underwater, as illustrated in Fig. 1, so the use of downhole sensors is extremely complex and expensive, and often practically unfeasible; this effectively limits the possible monitoring approaches to the analysis of the motor current, which is directly accessible from the surface. However, most ESPs use very high-power motors (up to hundreds of kilowatt), which make the effect of vibration less visible in the motor current.

The mechanical seal failure is known to be one of the main causes of premature failure of ESP, and excessive vibrations are often deemed responsible for this [17]–[21]. While a significant amount of research has been aimed at improving the design of the seal itself to enhance its robustness, an effective vibration monitoring would also be extremely helpful to achieve a timely detection of vibrations that could eventually lead to the mechanical seal failure. In particular, according

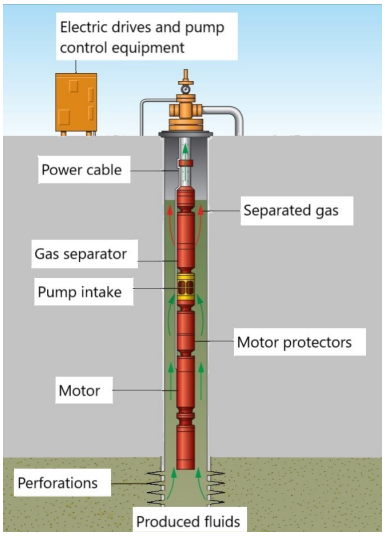

Figure 1. Schematic illustration of an electrical submersible pump (ESP).

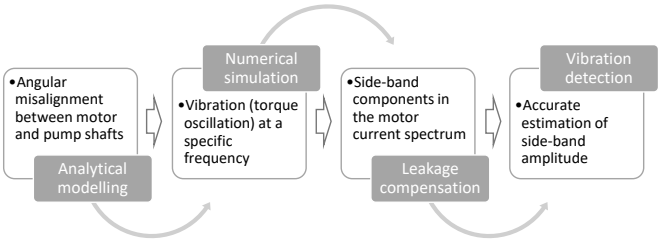

Figure 2. Block diagram of the research presented in this paper: The white blocks represent the conceptual steps that link the shaft misalignment to the amplitude of side-bands in the current spectrum; the gray blocks indicate the research methods adopted to analyse those links and achieve the final outcome of detecting the vibration.

to the literature, vibrations responsible for the seal failure are likely to be caused by a misalignment between the motor and pump shafts [22]. Therefore, this paper focuses on the motor current signature analysis to detect vibrations caused by shaft angular misalignment, although the proposed method has a wider applicability to the monitoring of different conditions.

The work includes analytical modelling, numerical simulations and experimental tests. A conceptual block diagram of the research is reported in Fig. 2, and the paper is accordingly structured as follows. Sec. II presents an analytical model to relate the shaft misalignment to motor torque oscillations and the appearance of side-band components in the current spectrum. Sec. III explains how the effect of spectral leakage can be significantly decreased, in order to achieve a much more accurate estimation of the amplitude of those side-band components in the current spectrum. Sec. IV reports the results of a simulation analysis, to illustrate the application of the proposed method. Finally, Sec. V reports the results of experimental tests carried out on a small-size motor, to confirm the validity of the method in real conditions.

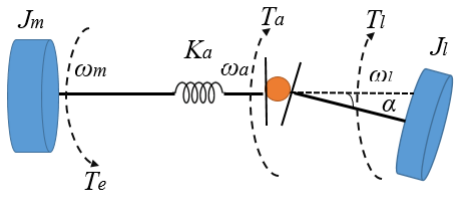

Figure 3. Flexible coupling model used to describe the effect of an angular misalignment between motor shaft and load shaft.

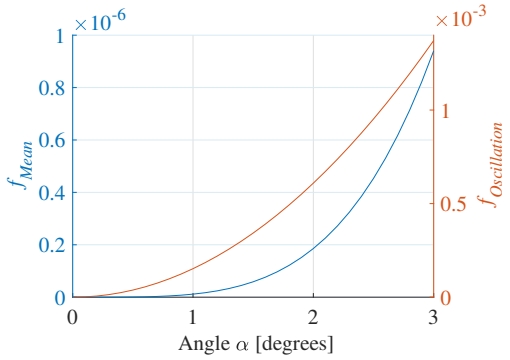

Figure 4. Increase in mean torque value (f_{Mean}) and amplitude of torque oscillation ($f_{\text{Oscillation}}$), as functions of the misalignment angle α, according to (7)-(10).

II. Effect of Vibrations on Motor Current

A. Effect of Shaft Misalignment on the Motor Torque

When the motor is connected to a mechanical load (such as the pump in the considered application), some level of misalignment between the two rotating shafts is likely to occur. The coupling employed to connect the two shafts usually allows for a small misalignment, without hindering the operation of the motor and the load. Nevertheless, the torque oscillations that appear because of this misalignment may cause vibrations that can eventually damage some sensitive mechanical components, such as the seal in the pump, and may lead to unexpected premature failure [23].

The flexible coupling model introduced by [24] and [25] is used to describe the effect of an angular misalignment on the induction motor. The model is illustrated in Fig. 3 and it is based on a universal joint with an elastic element, connected between the motor and load shafts. The motor is represented by its inertia J_{m}, angle θ_{m} and speed ω_{m}, while the load is similarly represented by its inertia J_{l}, angle θ_{l} and speed ω_{l}; the universal joint introduces the misalignment angle α, and the elastic element is represented by the elastic constant K_{a}.

The torque balance equation at the motor shaft can therefore be written as:

$$J_{\text{m}}\dot{\omega}_{\text{m}} = T_{\text{e}} - B_{\text{m}}\omega_{\text{m}} - T_{\text{a}} \tag{1}$$

where T_{e} is the electromagnetic torque produced by the motor and B_{m} is the dynamic friction coefficient. T_{a} is the load torque transferred to the motor shaft through the joint:

$$T_{\text{a}} = K_{\text{a}}\left(\theta_{\text{m}} - \theta_{\text{a}}\right) \tag{2}$$

where θ_{a} is related to the load angle by the following equation [25] (a full derivation of kinematic equations for a universal joint is reported in [26]):

$$\theta_{\text{a}} = \arctan\left(\frac{1}{\cos\alpha}\tan\theta_{\text{l}}\right) \tag{3}$$

Differentiating (3) with respect to time and applying trigonometric properties, the following relationship between the rotation speeds ω_{a} and ω_{l} is obtained:

$$\omega_{\text{a}} = \frac{d\theta_{\text{a}}}{dt} = \frac{1}{1+\frac{\tan^2\theta_{\text{l}}}{\cos^2\alpha}}\cdot\frac{1}{\cos\alpha}\cdot\frac{1}{\cos^2\theta_{\text{l}}}\cdot\frac{d\theta_{\text{l}}}{dt} = \\ = \frac{\cos\alpha}{1-\sin^2\alpha\cos^2\theta_{\text{l}}}\omega_{\text{l}} \tag{4}$$

Neglecting friction and damping effects in the joint, the mechanical power is transferred unchanged through the joint, therefore:

$$T_{\text{a}}\omega_{\text{a}} = T_{\text{l}}\omega_{\text{l}} \tag{5}$$

from which the following relationship is derived:

$$T_{\text{a}} = \frac{\omega_{\text{l}}}{\omega_{\text{a}}}T_{\text{l}} = \frac{1-\sin^2\alpha\cos^2\theta_{\text{l}}}{\cos\alpha}T_{\text{l}} \tag{6}$$

which can be rewritten as:

$$T_{\text{a}} = \left[\frac{1}{\cos\alpha} - \frac{\sin^2\alpha}{2\cos\alpha} - \left(\frac{\sin^2\alpha}{2\cos\alpha}\cos 2\theta_{\text{l}}\right)\right]T_{\text{l}} \tag{7}$$

Considering for simplicity a constant load torque T_{l}, which is a reasonable assumption in a short timescale, (7) shows that the misalignment has a double effect on the load torque transferred to the motor shaft: it slightly increases its mean value and it adds an oscillation at twice the load rotation frequency ω_{l}. This can be more explicitly seen by rewriting (7) as:

$$T_{\text{a}} = \left[1 + f_{\text{Mean}}(\alpha) - f_{\text{Oscillation}}(\alpha)\cos 2\theta_{\text{l}}\right]T_{\text{l}} \tag{8}$$

with:

$$f_{\text{Mean}}(\alpha) = \frac{1}{\cos\alpha} - \frac{\sin^2\alpha}{2\cos\alpha} - 1 \tag{9}$$

$$f_{\text{Oscillation}}(\alpha) = \frac{\sin^2\alpha}{2\cos\alpha} \tag{10}$$

The curves $f_{\text{Mean}}(\alpha)$ and $f_{\text{Oscillation}}(\alpha)$ are plotted in Fig. 4, which shows that the increase in the mean value of the torque is negligible and practically impossible to detect, whereas the torque oscillation (although small) can produce significant vibrations, which may eventually damage some mechanical components.

Such torque oscillation creates in turn an oscillation in the electromagnetic torque T_{e} produced by the motor, and it is therefore reflected into the motor current. By analysing the current signature, it is thus possible to identify and quantify the vibration.

B. Effect of Torque Oscillation on the Motor Current

The analysis of the effect of the torque oscillation derived in Sec. II-A on the motor current requires the formulation of a dynamic model of the motor, because the electrical quantities can no longer be described in terms of phasors. The dynamic model can be formulated by transforming all quantities on *dq* rotating axes, via the Park Transformation, as it is usually done for the analysis of the motor dynamic behavior. Neglecting the zero component, the three-phase windings are modeled in terms of two equivalent windings on two perpendicular axes d and q, rotating at synchronous speed, so the following four electrical equations are obtained for stator and rotor:

$$\begin{aligned}
\frac{dF_{\mathrm{qs}}}{dt} &= \omega_{\mathrm{e}}\left[V_{\mathrm{qs}} - F_{\mathrm{ds}} + \frac{R_{\mathrm{s}}}{x_{\mathrm{ls}}}\left(\frac{x_{\mathrm{m}}}{x_{\mathrm{lr}}}F_{\mathrm{qr}} + \left(\frac{x_{\mathrm{m}}}{x_{\mathrm{ls}}} - 1\right)F_{\mathrm{qs}}\right)\right] \\
\frac{dF_{\mathrm{ds}}}{dt} &= \omega_{\mathrm{e}}\left[V_{\mathrm{ds}} - F_{\mathrm{qs}} + \frac{R_{\mathrm{s}}}{x_{\mathrm{ls}}}\left(\frac{x_{\mathrm{m}}}{x_{\mathrm{lr}}}F_{\mathrm{dr}} + \left(\frac{x_{\mathrm{m}}}{x_{\mathrm{ls}}} - 1\right)F_{\mathrm{ds}}\right)\right] \\
\frac{dF_{\mathrm{qr}}}{dt} &= \omega_{\mathrm{e}}\left[-\frac{\omega_{\mathrm{e}} - \omega_{\mathrm{r}}}{\omega_{\mathrm{e}}}F_{\mathrm{dr}} + \frac{R_{\mathrm{r}}}{x_{\mathrm{lr}}}\left(\frac{x_{\mathrm{m}}}{x_{\mathrm{s}}}F_{\mathrm{qs}} + \left(\frac{x_{\mathrm{m}}}{x_{\mathrm{lr}}} - 1\right)F_{\mathrm{qr}}\right)\right] \\
\frac{dF_{\mathrm{dr}}}{dt} &= \omega_{\mathrm{e}}\left[-\frac{\omega_{\mathrm{e}} - \omega_{\mathrm{r}}}{\omega_{\mathrm{e}}}F_{\mathrm{qr}} + \frac{R_{\mathrm{r}}}{x_{\mathrm{lr}}}\left(\frac{x_{\mathrm{m}}}{x_{\mathrm{ls}}}F_{\mathrm{ds}} + \left(\frac{x_{\mathrm{m}}}{x_{\mathrm{lr}}} - 1\right)F_{\mathrm{dr}}\right)\right]
\end{aligned} \tag{11}$$

where ω_{e} is the electrical frequency, ω_{r} is the mechanical frequency multiplied by the pairs of poles, F are the normalised magnetic fluxes (multiplied by ω_{e}), V is the stator voltage, and R and x are the equivalent resistances and reactances of the motor.

The model is completed by the mechanical equation:

$$\frac{d\omega_{\mathrm{r}}}{dt} = \frac{p}{2}\frac{d\omega_{\mathrm{m}}}{dt} = \frac{p}{2J}\left(T_{\mathrm{e}} - T_{\mathrm{a}}\right) \tag{12}$$

where J is the overall inertia of the rotating system, p is the number of motor poles, T_{a} is the load torque on the motor shaft, expressed by (8), and T_{e} is the electromagnetic torque produced by the motor:

$$T_{\mathrm{e}} = \frac{3}{2}\frac{p}{2}\frac{1}{\omega_{\mathrm{e}}}\left(F_{\mathrm{ds}}i_{\mathrm{qs}} - F_{\mathrm{qs}}i_{\mathrm{ds}}\right) \tag{13}$$

The oscillations in the mechanical torque T_{a} produce small oscillations in the rotor speed, which in turn produce small oscillations in the fluxes and currents. The relationship between the torque oscillation and the flux oscillations, expressed by (11)-(13), is nonlinear. However, since all the oscillations are extremely small, the model can be linearized around the steady-state operating point of the motor. According to this approximation, a sinusoidal oscillation in T_{a} produces sinusoidal oscillations in both i_{ds} and i_{qs}, at the same frequency (i.e., twice the rotor mechanical frequency). Therefore the stator currents on *dq* axes can be written as:

$$\begin{aligned}
i_{\mathrm{ds}}(t) &= I_{\mathrm{ds}} + A_{\mathrm{ds}}\sin\left(2\omega_{\mathrm{m}}t + \theta_{\mathrm{ds}}\right) \\
i_{\mathrm{qs}}(t) &= I_{\mathrm{qs}} + A_{\mathrm{qs}}\sin\left(2\omega_{\mathrm{m}}t + \theta_{\mathrm{qs}}\right)
\end{aligned} \tag{14}$$

where $I_{\mathrm{ds,qs}}$ are the constant values corresponding to the steady-state operation, whereas $A_{\mathrm{ds,qs}}$ and $\theta_{\mathrm{ds,qs}}$ are the amplitudes and phases, respectively, of the oscillations calculated from the equivalent frequency response of the linearized model.

In order to analyze the effect of the oscillations in (14) on the three phase currents absorbed by the motor, the inverse Park Transformation can be applied:

$$[i_{abc}] = [P(\theta)]^{-1}[i_{dq0}] \tag{15}$$

where $P(\theta)$ is the Park Transformation matrix:

$$[P(\theta)] = \sqrt{\frac{2}{3}}\begin{bmatrix} \cos(\theta) & \cos(\theta - \frac{2\pi}{3}) & \cos(\theta - \frac{4\pi}{3}) \\ -\sin(\theta) & -\sin(\theta - \frac{2\pi}{3}) & -\sin(\theta - \frac{4\pi}{3}) \\ \frac{1}{\sqrt{2}} & \frac{1}{\sqrt{2}} & \frac{1}{\sqrt{2}} \end{bmatrix} \tag{16}$$

As the transformation considered here is on synchronous axes, the angle θ is the electrical angle $\theta(t) = \int_0^t \omega_{\mathrm{e}}dt = \omega_{\mathrm{e}}t$ (assuming the electrical frequency to be constant in this analysis).

The three phases of the motor behave in a similar way (apart from the phase shift), so the inverse Park Transformation is reported here only for the current of the first phase for sake of simplicity:

$$\begin{aligned}
i_a(t) = &\sqrt{\frac{2}{3}}\cos(\omega_e t)\left[I_{ds} + A_{ds}\sin(2\omega_m t + \theta_{ds})\right] + \\
&-\sqrt{\frac{2}{3}}\sin(\omega_e t)\left[I_{qs} + A_{qs}\sin(2\omega_m t + \theta_{qs})\right]
\end{aligned} \tag{17}$$

The expression in (17) shows that the current waveform contains the fundamental component at the electrical frequency ω_{e}, corresponding to the normal operation of the motor, with the addition of other two components at frequencies $\omega_{\mathrm{e}} - 2\omega_{\mathrm{m}}$ and $\omega_{\mathrm{e}} + 2\omega_{\mathrm{m}}$, which are created by the torque oscillation, in turn created by the misalignment angle α. The analysis of the current spectrum in the frequency domain is therefore expected to reveal two side-bands at those frequencies, whose amplitudes can be related to the amplitude of the torque oscillation and, from that, to the misalignment. However, the amplitudes of those side-bands are usually much smaller (several orders of magnitudes) than the amplitude of the main component, so their accurate measurement presents important challenges, particularly arising from the spectral leakage in non-synchronous sampling conditions. A method to compensate for the leakage error is presented in the next section.

III. Leakage Error Compensation Method

The spectrum of a signal, calculated by applying the Fourier Transform, is affected by spectral leakage when the observation window does not include an integer number of periods of the signal. This condition is called non-synchronous sampling, and it is likely to occur when a fixed sampling window is used to acquire a signal with an unknown (or time-varying) frequency. This is likely to be the case in the considered application, as the electrical frequency of the motor continuously changes over time, due to the changes in the power supply frequency or according to the drive control algorithm.

The leakage error is particularly severe when a short observation window is used, because of the corresponding poor frequency resolution of the calculated spectrum. However, a

short window is required when the system is not in steady-state conditions, in order to limit the changes that occur during that time window, which may jeopardize the validity of the Fourier analysis if they are not negligible. The choice of the optimal time window is therefore usually a trade-off between the need to keep the leakage low and the need to keep the transients in the signal limited. Nevertheless, even a small leakage can completely hinder the detection of the small side-band components in the motor current spectrum analysis, for the vibration monitoring considered in this paper. Hence, a method for leakage error compensation is proposed, explained in this section.

Owing to the linearity of the Fourier Transform, the superposition principle applies and so the effects of spectral leakage can be analyzed on each frequency component of the signal independently. Therefore, a sinusoidal signal can be considered in the following, without loss of generality:

$$s\left(t\right) = A\sin\left(\omega^* t + \phi\right) \tag{18}$$

where ω^* is a known frequency.

When the signal is acquired over a window $w(t)$ and then transformed into the frequency domain according to the Fourier Transform, the resulting spectrum $P(j\omega)$ is the convolution between the ideal signal spectrum $S(j\omega)$ and the window spectrum $W(j\omega)$:

$$P(j\omega) = S(j\omega) * W(j\omega) \tag{19}$$

In case of a rectangular window, defined by N samples acquired with sampling time T_s and assumed to be symmetrical with respect to the time origin, the window spectrum is:

$$W(j\omega) = \frac{\sin\left(\frac{\omega}{2}NT_s\right)}{\sin\left(\frac{\omega}{2}T_s\right)} \tag{20}$$

which is a real periodic function, with period $2\pi/T_s$. The convolution step, $2\pi/(NT_s)$, is equal to the frequency resolution of the measured signal spectrum $P(j\omega)$. Therefore, $P(j\omega)$ is defined only at discrete frequencies $2\pi h/(NT_s)$, where h is an integer number (harmonic number).

The calculation of $P(j\omega)$ according to (19) is illustrated in Fig. 5. If the signal frequency is an integer multiple of the frequency resolution, only two non-zero elements will appear in $P(j\omega)$, at the same frequency of the signal (positive and negative), as in all other convolution steps the two spectral lines in $S(j\omega)$ will fall on the zero crossings of $W(j\omega)$; this condition corresponds to the synchronous sampling, and no leakage error occurs. On the contrary, if this condition is not satisfied, the result of the convolution will be different from zero at each convolution step, and the power of the signal will be spread across the whole frequency axis, as illustrated in Fig. 5; this is the spectral leakage.

The idea underlying the proposed method is that, for a sinusoidal signal at a given frequency ω^* and a known observation window (defined by N and T_s), the effect of spectral leakage is predictable, as it arises from the convolution in (19). It is therefore possible to compensate for the leakage error in the measured spectrum, by using a model-based fitting of $P(j\omega)$. In more detail, for each discrete frequency component h, the

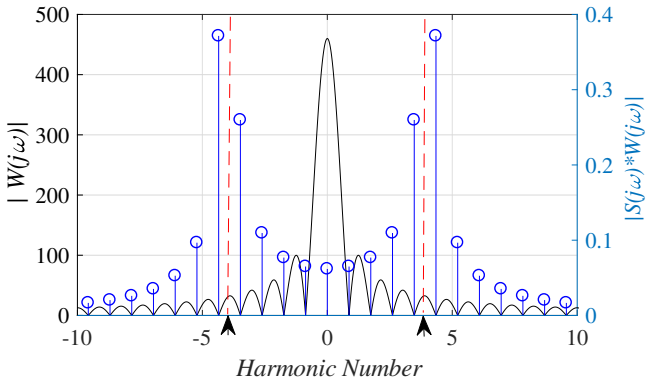

Figure 5. Illustration of the spectral leakage arising from (19) in case of non-synchronous sampling: the red lines represent the ideal signal spectrum $|S(j\omega)|$, the black curve is the spectrum of the window $|W(j\omega)|$ and the blue spectrum is the resulting signal spectrum $|P(j\omega)| = |S(j\omega) * W(j\omega)|$.

spectrum $P(h)$ can be written as a function of the amplitude A and phase ϕ of the sinusoidal signal in (18):

$$P(h) = \frac{A}{2N}\left(W_+(h)e^{j\phi} + W_-(h)e^{-j\phi}\right)e^{-j\pi h} \tag{21}$$

where:

$$W_+(h) = \frac{\sin((h^* - h)\pi)}{\sin((h^* - h)\pi/N)} \tag{22}$$

$$W_-(h) = \frac{\sin((h^* + h)\pi)}{\sin((h^* + h)\pi/N)} \tag{23}$$

and $h^* = \omega^* NT_s/(2\pi)$ is the non integer harmonic number corresponding to the signal frequency ω^*.

This approach can be used to compensate for the spectral leakage in the motor current spectrum, particularly when calculated from a short observation window. The motor current waveform is dominated by the electrical frequency component, and therefore it can be well approximated by a sinusoidal signal like (18). If the electrical frequency is known, which may be the case if it is controlled by a motor drive synchronized with the signal acquisition, then the functions $W_+(h)$ and $W_-(h)$ are known, and the spectrum can be fitted according to the model in (21) to estimate A and ϕ, with a very limited computational effort. If the electrical frequency is not known, it can be estimated together with A and ϕ from the same model; the computational effort will be larger, and the accuracy of the results may be slightly worse, but the same method can still be applied.

Once the amplitude, frequency and phase of the dominant sinusoidal component have been estimated, the spectral leakage is completely determined and it can be removed from the spectrum, in order to improve the estimation of the amplitudes of the other (smaller) frequency components in the spectrum that were significantly affected by the leakage error. A similar approach was adopted in [16] for the detection of broken rotor bar faults in induction motors, which create characteristic side-bands in the current spectrum. The application considered in this paper, however, presents additional challenges because of the much lower vibration levels, more difficult to detect, which require dedicated solutions for the model-based fitting

of the spectrum. The proposed method is illustrated in the next two sections, by means of simulation and experimental tests, respectively. Designing an experimental setup to induce a controlled misalignment is a challenging task by itself, and it represents another significant novelty compared to [16].

IV. Simulation Results

The model presented in Sec. II was implemented in Matlab Simulink, to simulate the motor current waveform obtained with different misalignment angles, different electrical frequencies and different rotation speeds. A wide range of motor power ratings was considered for the simulation, to reflect the wide range of motors employed in electrical submersible pump applications, and to validate the proposed method at different power levels. Two cases (4 kW and 37 kW) are reported in this section.

All simulations were based on 4-poles motors and were run with a constant electrical frequency and a constant motor rotation speed (apart from the small oscillations induced by the torque oscillation). A misalignment angle of 0.5° was chosen for the simulation, to consider a realistic example. According to (10), the torque oscillation amplitude produced in this condition is expected to be around $3.8 \cdot 10^{-5}$ times the mean torque value. It is therefore very difficult to measure accurately, or even just to detect, from the current spectrum analysis.

A. Simulation of 4 kW Induction Motor

The first considered case study is based on a 4 kW motor. The electric power supply is a positive-sequence three-phase voltage, with a constant electrical frequency equal to f_e = 49.6 Hz. The load torque was chosen in order to have a rotor speed (mean value) f_m = 23.85 Hz. According to the analysis reported in Sec. II, the misalignment is expected to produce two side-bands in the current spectrum at frequencies $f_e - 2f_m$ = 1.9 Hz and $f_e + 2f_m$ = 97.3 Hz.

The proposed method is illustrated considering a time window of 2.4 s, which is not synchronous with the electrical frequency (it contains 119.04 periods of the current component at the electrical frequency). As a consequence, the current spectrum is affected by leakage of the electrical frequency component, in addition to a much smaller leakage of the side-band components. Although the leakage of the electrical component is not particularly significant in this case (as the deviation from synchronous condition is small), it is still largely dominant over the side-band components. This means that the approximation of the spectrum with that of a sinusoidal signal is well justified and the fitting method proposed in Sec. III can be applied.

The calculated current spectrum is shown in Fig. 6, in the range from 3 Hz to 96 Hz, thus excluding a narrow frequency range (3-Hz wide) around each side-band, in order to avoid any possible significant contribution from the side-bands. The spectrum in this range is produced by the current component at f_e only, and it can therefore be fitted by the model presented in Sec. III to estimate the amplitude and phase of that component. As the peak value of the spectrum in Fig. 6 is more than 1000

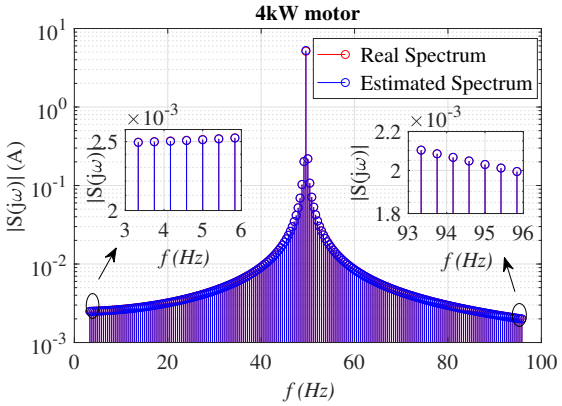

Figure 6. Magnitude of the current spectrum calculated from the current signal acquired over 2.4 s (red), compared to the best fit (blue) obtained from the model presented in Sec. III, based on a sinusoidal signal.

times higher than the values at the two sides, a traditional least-square-error fitting over the whole frequency range could lead to a poor fitting at the extreme parts of the spectrum (near the side-bands). Hence, a narrower frequency range is proposed to achieve a better fitting locally; e.g., for the left side of the spectrum, a range from 3 Hz to 30 Hz was chosen. The best fit thus obtained is also plotted in Fig. 6 and it shows an excellent agreement with the actual spectrum in the whole frequency range.

The knowledge of the amplitude and phase of the electrical frequency component in the current, estimated from the spectrum fitting, allows removing that component from the spectrum (including its leakage), thus revealing the side-bands which were originally completely hidden by the spectral leakage of the electrical frequency component. The residual spectrum is shown in Fig. 7, in a frequency range around the 1.9 Hz side-band, which is the smallest of the two side-bands and therefore also the most difficult one to estimate. It is worth noting that the residual spectrum shown in Fig. 7 has an amplitude that is three orders of magnitude lower than the original spectrum shown in Fig. 6, in the same frequency range. Although this spectrum may still be affected by some other residual frequency components, the side-band is now visible and its amplitude can be estimated by using again the model-based fitting method presented in Sec. III, this time in the range from 0 to 3 Hz. The best fit is also plotted in Fig. 7, and the estimated side-band amplitude is reported in Table I, compared to a benchmark value obtained from the analysis of the same current signal carried out on a synchronous 20 s window, characterized by no spectral leakage of the electrical frequency component. The estimated amplitudes of the other side-band and the electrical frequency component are also reported in Table I for sake of completeness. The results show that the proposed method can estimate the side-band amplitudes with a satisfactory level of accuracy, which is quite remarkable considering that they are between five and six orders of magnitude lower than the amplitude of the electrical frequency component.

It is worth comparing the proposed leakage compensation method to a more common approach, based on the use of

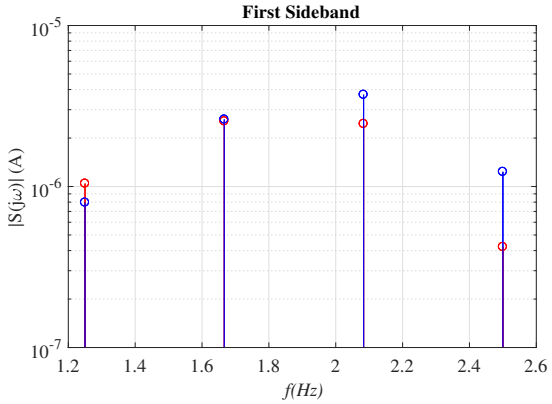

Figure 7. Magnitude of the current spectrum without the electrical frequency component (red), compared to the best fit (blue) to estimate the amplitude of the 1.9 Hz side-band.

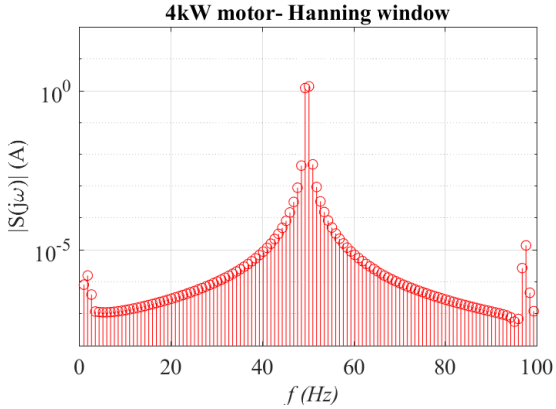

Figure 8. Magnitude of the current spectrum calculated from the current signal acquired over 2.4 s (red), after the application of a 2^{nd}-order Hanning window.

Table I
AMPLITUDES OF THE CURRENT COMPONENTS (4 KW MOTOR)

Frequency	Estimated amplitude with 20 s window (without leakage)	Estimated amplitude with 2.4 s window (with leakage)
f_e = 49.6 Hz	5.127 A	5.125 A
f_{s1} = 1.9 Hz	7 μA	10 μA
f_{s2} = 97.3 Hz	35 μA	35 μA

Table II
AMPLITUDES OF THE CURRENT COMPONENTS (37 KW MOTOR)

Frequency	Estimated amplitude with 20 s window (without leakage)	Estimated amplitude with 2.4 s window (with leakage)
f_e = 49.6 Hz	42.14 A	42.14 A
f_{s1} = 0.6 Hz	47 μA	50 μA
f_{s2} = 98.6 Hz	120 μA	120 μA

non-rectangular windows, which are known to decrease the spectral leakage in non-synchronous sampling conditions. The recommended procedure to apply a n-th order window is by increasing the sampling window length by n times, in order to keep the same frequency resolution in the resulting spectrum. This is, however, not appropriate in those applications that require a short window to avoid significant transients within the window itself. The alternative option is, therefore, keeping the same window length and enlarging the frequency resolution by n times. The resulting spectrum for the current signal considered above is reported in Fig. 8, after the application of a 2^{nd}-order Hanning (also known as Hann) window, which is a common choice to decrease long-range leakage [15]. The window length is still 2.4 s, as before, which means that the frequency resolution is now double. Fig. 8 shows that the long-range leakage is greatly reduced, and the two side-bands become visible. However, the worsened frequency resolution may affect the accuracy of the side-band amplitude estimation and, in some cases, it may not be enough to allow distinguishing the side-band at all. The use of non-rectangular windows, therefore, may work well in many cases, but it is not always appropriate because it affects the trade-off between short time window and good frequency resolution, which is of critical importance in the considered application.

B. Simulation of 37 kW Induction Motor

The second considered case study is based on a 37 kW motor, powered by the same voltage supply as the 4 kW motor; therefore, the absorbed current is almost ten times higher than in the previous case. This case study is chosen to illustrate the challenges that arise from higher-current motors, which make the side-bands caused by the misalignment less visible and more difficult to estimate, as their amplitudes do not increase proportionally to the main current component (for a given misalignment angle).

The electrical frequency f_{e} is kept at 49.6 Hz as before, whereas the mechanical frequency is now f_{m} = 24.5 Hz. The expected side-bands are therefore at 0.6 Hz and 98.6 Hz. The same methodology described in Sec. IV-A is followed to estimate the amplitudes of those side-band components, and the results are reported in Table II. The proposed method can still provide very accurate results, despite the fact that the relative amplitude of the side-bands compared to the main current component is now slightly smaller than in the previous case, as expected.

V. EXPERIMENTAL RESULTS

A. Experimental Setup

In order to experimentally validate the proposed method for the leakage error compensation in motor current signature analysis, a test rig was specifically designed to allow introducing a small and controlled misalignment between the motor and load shafts. A 1.5 kW three-phase, 2-poles induction motor was employed, whose power rating is comparable to the 4 kW motor used in the simulation analysis in the previous section. The nature of the experiment required keeping the power limited to avoid potentially dangerous vibrations.

This motor was connected to another identical motor, used as a generator, in order to create the mechanical load for the motor. The two shafts were connected through an elastic jaw coupling to re-create the same conditions used to formulate the misalignment model in Sec. II. The generator was connected to a variable resistor bank, designed to allow testing the motor at 0%, 25%, 50%, 75%, or 100% of its rated power.

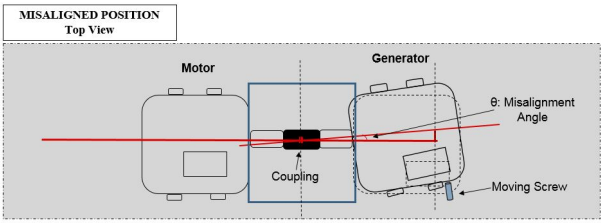

(a)

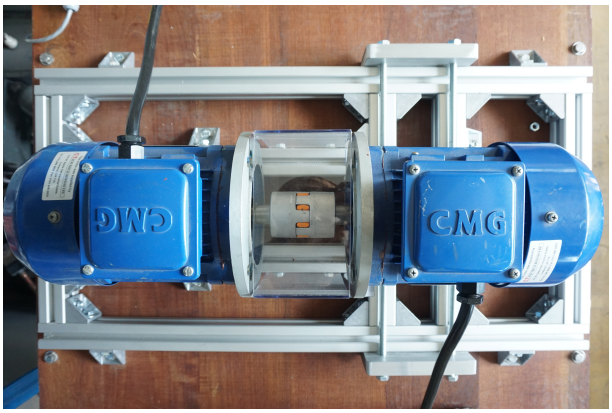

(b)

Figure 9. Schematic illustration (a) and photograph (b) of the motor-generator assembly used for the experimental tests, with a specifically-designed mechanism to create an angular misalignment between the motor and generator shafts.

The test rig was designed in such a way to allow moving the generator sideways at its rear end, by means of a moving screw, while the motor remains in a fixed position. This mechanism allows creating an angular misalignment between the motor and load shafts, up to a few degrees. A schematic illustration of this design and a photograph of the whole assembly are shown in Fig. 9. Knowing the distance between the coupling and the rear movable feet of the generator (24 cm), the misalignment angle can be calculated and controlled by measuring the lateral movement allowed by the moving screw, according to simple trigonometric calculations on the right-angled triangle illustrated in Fig. 9(a).

The three phase currents absorbed by the motor are measured by three closed-loop Hall-effect current transducers (LEM LA 25-P), which have an accuracy below 1% and a bandwidth from DC to 200 kHz. The voltage signals from the transducers outputs are acquired by a 4-channel, 16-bit data acquisition board (National Instruments 9125), with 100 kHz simultaneous sampling.

B. Current Measurements

Before commenting on the experimental results, it should be noted that the real operation of the motor is more complex than the simulated behavior reported in Sec. IV, and the current spectrum is therefore likely to contain a number of components in addition to the expected side-bands according to the model in Sec. II, but they are all affected by the spectral leakage of the main component at the electrical frequency, so the method proposed in this paper can still be applied to better estimate

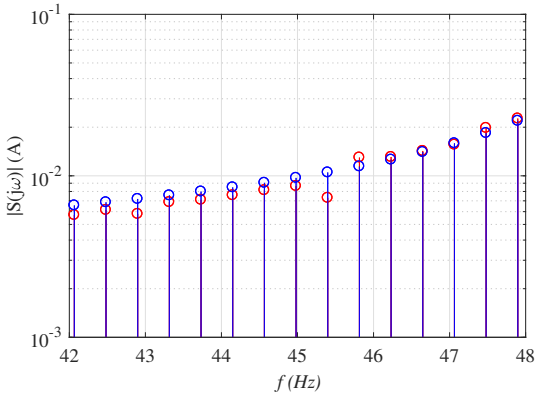

Figure 10. Magnitude of the current spectrum calculated from the measured current over 2.4 s (red), with 0.5° misalignment, compared to the best fit (blue) obtained from the model presented in Sec. III.

the amplitudes of all those side-bands. It should also be noted that the motor used for the experimental tests has 2 poles, whereas the one used in the simulations had 4 poles, so the expected side-bands at frequencies $f_e \pm 2f_m$ will be in different positions. An estimate of those frequencies in rated conditions can be calculated from the rated electrical frequency (50 Hz) and the rated speed (2860 RPM, i.e. 47.7 Hz): therefore, the expected side-bands are around 45.4 Hz and 145.4 Hz.

The first test was carried out with an estimated angular misalignment of 0.5°, as in the simulations presented in Sec. IV. The spectrum of the current in one phase, calculated again in a 2.4 s acquisition window, is reported in Fig. 10, in a range from 42 to 48 Hz. The effect of the spectral leakage from the electrical frequency component is evident, and such a leakage affects the appearance of the side-band component around 45.4 Hz, whose amplitude cannot be accurately estimated from this spectrum. A similar procedure as described in Sec. IV is then followed again here to remove the electrical frequency component and its leakage from the spectrum, with the difference that now f_e is unknown. The frequency range chosen for the local fitting is 42-48 Hz, except for the narrower range 45-46.5 Hz, which is expected to be affected by the side-band. The best fit of the spectrum with the model in Sec. III is plotted in Fig. 10, and it shows a very good agreement with the measured spectrum, apart from the narrow frequency range around the side-band, as expected.

The residual spectrum after the removal of the estimated contribution from the electrical frequency component is plotted in Fig. 11, together with its best fit based again on the model in Sec. III. The estimated frequencies and amplitudes of this side-band and the electrical frequency component are reported in Table III and compared to the same quantities estimated from a 20 s observation time (while running the motor in steady-state conditions). The results confirm that the proposed method can provide accurate estimates of the side-band amplitudes also in real experimental scenarios.

The same analysis was repeated on the current signal acquired from a second test, carried out with a slightly higher misalignment angle of 0.7°. The estimated side-band amplitude in this case is also reported in Table III, and

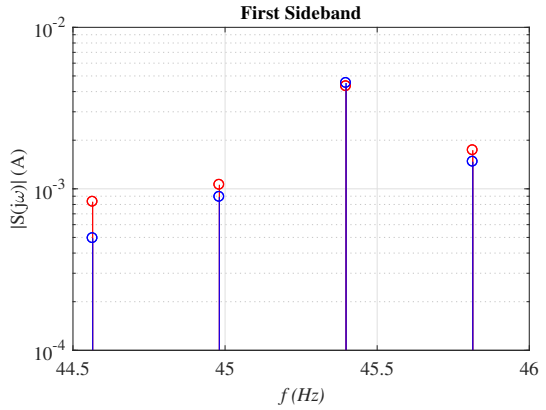

Figure 11. Magnitude of the measured current spectrum shown in Fig. 10, without the electrical frequency component (red), compared to its best fit (blue) to estimate the side-band amplitude.

Table III
AMPLITUDES OF THE CURRENT COMPONENTS (EXPERIMENT)

α = 0.5°

Expected frequency	Estimated amplitude with 20 s window (negligible leakage)	Estimated amplitude with 2.4 s window (with leakage)
f_e = 50 Hz	3.55 A	3.6 A
f_{s1} = 45.4 Hz	10 mA	10 mA

α = 0.7°

Expected frequency	Estimated amplitude with 20 s window (negligible leakage)	Estimated amplitude with 2.4 s window (with leakage)
f_e = 50 Hz	3.58 A	3.61 A
f_{s1} = 45.4 Hz	14.2 mA	15 mA

it reveals again a good estimation accuracy. Moreover, this result also confirms that this side-band is associated with the misalignment, and its amplitude increases as the misalignment grows, as expected. Hence, measuring the side-band amplitude can be effectively used to monitor the misalignment-induced vibrations.

VI. CONCLUSIONS

This paper proposed a method to compensate for the spectral leakage that is likely to affect motor current signature analysis, when a short time window is employed for the Fourier transformation in order to satisfy the steady-state condition requirements. The method is based on the assumption that the dominant component of the current waveform is a sine wave at the electrical frequency, whose amplitude and phase (and frequency, if not known) can be accurately estimated through a model-based fitting of the measured spectrum. The dominant leakage caused by this component can thus be removed from the spectrum, in order to make other components more visible and measurable.

In particular, this method was successfully applied to the estimation of side-band frequency components caused by vibrations induced by a small angular misalignment between the motor and load shafts. A model to describe the effect of such a misalignment was firstly formulated, and then the proposed method was validated through simulation and experimental tests. The results confirm the effectiveness of the method to estimate the amplitudes of side-bands that are several orders of magnitude smaller than the main current component and would be invisible in the original spectrum.

The accuracy of the amplitude estimation depends on a number of factors, including the power rating of the motor, the level of vibrations, the presence of other side-band components and noise in the current spectrum, and the length of the window used for the spectrum calculation, which in turn depends on the timescale of the expected variations in the operating conditions (supply frequency, motor speed, torque, etc.). All those aspects should be carefully evaluated in future analysis, in order to establish the feasibility of the proposed method for a specific industrial application. A detailed characterization should also be carried out for each application, through either simulation or experimental tests, to obtain the empirical relationship between the misalignment angle and the amplitudes of the characteristic side-bands in the current spectrum, which is required to estimate the misalignment from the side-band measurement.

REFERENCES

[1] S. Güçlü, A. Ünsal, and M. A. Ebeoğlu, "Vibration analysis of induction motors with unbalanced loads," in *10th International Conference on Electrical and Electronics Engineering (ELECO)*, 2017, pp. 365–369.

[2] V. P. Raj, K. Natarajan, and S. T. Girikumar, "Induction motor fault detection and diagnosis by vibration analysis using mems accelerometer," in *International Conference on Emerging Trends in Communication, Control, Signal Processing and Computing Applications (C2SPCA)*, 2013, pp. 1–6.

[3] L. Eren and M. J. Devaney, "Bearing damage detection via wavelet packet decomposition of the stator current," *IEEE Transactions on Instrumentation and Measurement*, vol. 53, no. 2, pp. 431–436, 2004.

[4] A. Sadeghian, Z. Ye, and B. Wu, "Online detection of broken rotor bars in induction motors by wavelet packet decomposition and artificial neural networks," *IEEE Transactions on Instrumentation and Measurement*, vol. 58, no. 7, pp. 2253–2263, July 2009.

[5] R. Puche-Panadero, M. Pineda-Sanchez, M. Riera-Guasp, J. Roger-Folch, E. Hurtado-Perez, and J. Perez-Cruz, "Improved resolution of the mcsa method via hilbert transform, enabling the diagnosis of rotor asymmetries at very low slip," *IEEE Transactions on Energy Conversion*, vol. 24, no. 1, pp. 52–59, January 2009.

[6] Z. Ye, B. Wu, and A. Sadeghian, "Current signature analysis of induction motor mechanical faults by wavelet packet decomposition," *IEEE Transactions on Industrial Electronics*, vol. 50, no. 6, pp. 1217–1228, Dec 2003.

[7] H. Douglas, P. Pillay, and A. K. Ziarani, "A new algorithm for transient motor current signature analysis using wavelets," *IEEE Transactions on Industry Applications*, vol. 40, no. 5, pp. 1361–1368, September 2004.

[8] T. Yang, H. Pen, Z. Wang, and C. S. Chang, "Feature knowledge based fault detection of induction motors through the analysis of stator current data," *IEEE Transactions on Instrumentation and Measurement*, vol. 65, no. 3, pp. 549–558, March 2016.

[9] F. Blaabjerg, J. K. Pedersen, E. Ritchie, and P. Nielsen, "Determination of mechanical resonances in induction motors by random modulation and acoustic measurement," *IEEE transactions on industry applications*, vol. 31, no. 4, pp. 823–829, July 1995.

[10] P. Rzeszucinski, M. Orman, C. T. Pinto, A. Tkaczyk, and M. Sulowicz, "Bearing health diagnosed with a mobile phone: Acoustic signal measurements can be used to test for structural faults in motors," *IEEE Industry Applications Magazine*, vol. 24, no. 4, pp. 17–23, July 2018.

[11] A. Glowacz, W. Glowacz, Z. Glowacz, and J. Kozik, "Early fault diagnosis of bearing and stator faults of the single-phase induction motor using acoustic signals," *Measurement*, vol. 113, pp. 1–9, July 2018.

[12] T. Yamada, "High-accuracy estimations of frequency, amplitude, and phase with a modified dft for asynchronous sampling," *IEEE Transactions on Instrumentation and Measurement*, vol. 62, no. 6, pp. 1428–1435, 2013.

[13] S. Tomar and P. Sumathi, "Amplitude and frequency estimation of exponentially decaying sinusoids," *IEEE Transactions on Instrumentation and Measurement*, vol. 67, no. 1, pp. 229–237, 2017.

[14] M. A. Platas-Garza and J. A. de la O Serna, "Dynamic harmonic analysis through taylor–fourier transform," *IEEE Transactions on Instrumentation and Measurement*, vol. 60, no. 3, pp. 804–813, 2010.

[15] G. D'Antona and A. Ferrero, *Digital signal processing for measurement systems: theory and applications*. Springer Science & Business Media, 2005.

[16] N. Afrizal, R. Ferrero, and S. Toscani, "Leakage error compensation in induction motor current measurements for rotor fault diagnosis," in *2016 IEEE International Workshop on Applied Measurements for Power Systems (AMPS), Aachen, Germany*, 28-30 October 2016, pp. 1–6.

[17] J. Selvakumar and K. Natarajan, "Failure analysis of centrifugal pumps based on survey," *ARPN Journal of Engineering and Applied Sciences*, vol. 10, no. 4, pp. 1960–1965, September 2015.

[18] J. Xiao, R. Shepler, Y. Windiarto, S. Parkinson, R. Fox *et al.*, "Development and field test of esp reliable power delivery system," in *SPE Kingdom of Saudi Arabia Annual Technical Symposium and Exhibition*. Society of Petroleum Engineers, 2016.

[19] D. Childs, C. Norrbin, and S. Phillips, "A lateral rotordynamics primer on electric submersible pumps (esps) for deep subsea applications," in *43rd Pump and Turbomachinery Symposia, Houston, TX*, September 2014, pp. 23–25.

[20] S. Sawaryn, E. Ziegel *et al.*, "Statistical assessment and management of uncertainty in the number of electric-submersible pump failures in a field," in *SPE Annual Technical Conference and Exhibition*, 2001.

[21] W. D. Marscher *et al.*, "Avoiding failures in centrifugal pumps," in *Proceedings of the 19th International Pump Users Symposium*, 2002, pp. 157–166.

[22] M. Tsypkin, "Induction motor condition monitoring: Vibration analysis technique - a practical implementation," in *2011 IEEE International Electric Machines Drives Conference (IEMDC)*, May 2011, pp. 406–411.

[23] B. Corne, J. Knockaert, and J. Desmet, "Misalignment and unbalance fault severity estimation using stator current measurements," in *IEEE 11th International Symposium on Diagnostics for Electrical Machines, Power Electronics and Drives, SDEMPED*, October 2017, pp. 247–253.

[24] C. Verucchi, J. Bossio, G. Bossio, and G. Acosta, "Misalignment detection in induction motors with flexible coupling by means of estimated torque analysis and mcsa," *Mechanical Systems and Signal Processing*, vol. 80, pp. 570–581, December 2016.

[25] J. M. Bossio, G. R. Bossio, and C. H. De Angelo, "Angular misalignment in induction motors with flexible coupling," in *35th Annual Conference of IEEE Industrial Electronics*, 2009, pp. 1033–1038.

[26] M. Xu and R. Marangoni, "Vibration analysis of a motor-flexible coupling-rotor system subject to misalignment and unbalance, part i: theoretical model and analysis," *Journal of sound and vibration*, vol. 176, no. 5, pp. 663–679, 1994.

Nurafnida Afrizal received her PhD degree in Electrical Engineering from University of Liverpool, UK, in 2020. She is part of the young academic training scheme staff at the School of Ocean Engineering, Universiti Malaysia Terengganu (UMT), Malaysia. Her research interests include the development of methods and algorithms for signal processing in condition monitoring of the electrical machine particularly in marine application.

Roberto Ferrero (S10-M14-SM18) received his PhD degree (cum laude) in Electrical Engineering from Polytechnic of Milan, Italy, in 2013. From 2015 to 2019 he was a Lecturer with the Department of Electrical Engineering and Electronics, University of Liverpool, UK, where he is currently a Senior Lecturer (Associate Professor). His main research activity is focused on electrical measurements, particularly applied to power systems and electrochemical devices. He is a member of the IEEE Instrumentation and Measurement Society, and of its TC 39 (Measurements in Power Systems). He has been an Associate Editor of the IEEE Transactions on Instrumentation and Measurement since 2017.